Atmospheric Environment 207 (2019) 52–62

Contents lists available at ScienceDirect

Atmospheric Environment

journal homepage: www.elsevier.com/locate/atmosenv

Impact of aerosols of sea salt origin in a coastal basin: Sydney, Australia

Jagoda Crawford*, David D. Cohen, Scott D. Chambers, Alastair G. Williams, Armand Atanacio

ANSTO, Locked Bag 2001 Kirrawee DC, NSW, 2232, Australia

ARTICLE INFO

Keywords:
Fine particles
Positive matrix factorisation
Sea salt
Secondary sulfate

ABSTRACT

Sea salt is one of the major aerosols in the atmosphere in both the fine and coarse size ranges. Newly formed sea salt particles have a similar composition to seawater; including elements such as Na, Cl, Mg, S, Ca, Br and K. However, once in the atmosphere sea salt particles can undergo chemical reactions with other airborne pollutants, resulting in a loss of chlorine (whereas Na is conservative). The modified aerosol is commonly referred to as aged sea spray or aged sea salt.

Fine aerosols from two sites in the Sydney Basin were analysed for source fingerprints with components that may have originated from the ocean (i.e. fresh and aged sea spray). At Lucas Heights, 18.4 km from the nearest coast, the average source fingerprint concentrations of fresh and aged sea spray were 0.47 ± 0.02 and 1.08 ± 0.03 μg/m^3, respectively. At Richmond, 58 km from the coast, the average fingerprint concentrations of fresh and aged sea spray were 0.26 ± 0.01 and 0.87 ± 0.02 μg/m^3, respectively. At Lucas heights, fresh and aged sea spray contributed to 11% and 21% of $PM_{2.5}$, respectively. At Richmond fresh and aged sea spray contributed to 4.8 ± 0.35 and 16 ± 0.5% of the $PM_{2.5}$, respectively.

The Cl/Na ratios of aged sea spray at Lucas Heights and Richmond were 0.72 and 0.87, respectively, in comparison to 1.54 for fresh sea salt. At Richmond the corresponding Ca/Na and K/Na ratios were both 0.037 (close to that of seawater), and at Lucas Heights, the corresponding ratios were 0.038 and 0.026, respectively.

Back trajectory and Radon-222 analysis demonstrated that the largest concentrations of aged sea spray occur when the air masses had travelled over regions of anthropogenic sources. This confirms an interaction between anthropogenic precursors and sea spray that liberates chlorine enabling it to contribute to other chemical reactions in the atmosphere, e.g. resulting in an increase in the formation of ozone.

1. Introduction

Sea salt is one of the major aerosols in the atmosphere both in the fine and coarse size ranges (Prijith et al., 2014). The rate of sea salt aerosol formation (usually represented by the atmospheric columnar aerosol optical depth; AOD) has been found to follow a linear relationship with ocean surface wind speeds (slope = 0.0053 AOD day^{-1}m^{-1}s, intercept = 0.0163 AOD day^{-1}; Prijith et al., 2014). Newly formed sea salt particles have effectively the same composition as seawater; including elements such as Na, Cl, Mg, S, Ca, Br and K (Adachi and Buseck, 2015; and references therein). Once in the atmosphere sea salt particles undergo chemical reactions resulting in loss of chlorine to the gaseous phase (Pio and Lopes, 1998; Song and Carmichael, 1999). This chloride loss is attributed to reactions with chemicals such as SO_2, H_2SO_4 and NHO_3, which result in the de-gassing of HCl, or interactions with NO_2, N_2O_5, HOBr and O_3, which result in the release of NOCl, HONO, $ClNO_2$, Cl_2 and BrCl (Pio and Lopes, 1998 and references therein). After chlorine depletion Na and Mg (which are conservative) can be used as tracers of aged sea salt (i.e. Cl depleted sea salt; Adachi and Buseck, 2015) and in particular the Cl/Na ratio is a good measure of the extent of Cl depletion (Foltescu et al., 1996). Furthermore, higher percentage of Cl depletion appears to occur in the fine aerosol fraction (Feng et al., 2017).

Some initial chlorine depletion of the sea salt aerosol can take place near the coast and over the ocean due to interactions with dimethyl sulphide (DMS). DMS, linked to phytoplankton dynamics, is emitted into the atmosphere shortly after production and subsequently undergoes a sequence of gas phase oxidation reactions, the products of which, in turn, react with sea salt aerosols (Hopkins et al., 2008). However, chlorine depletion near the coast due to DMS is far less than that attributable to reactions with anthropogenic emissions (Quinn and Bates, 2005). Gondwe at al. (2003), using version 3 of the 3-D global Chemical Transport Model (Tracer Model 3), estimated that in the Sydney Basin the maximum contribution from DMS to SO_4^-, over the vertical column, to be in the order of 25%. The displacement of chloride from sea spray in a coastal environment subsequently affects ozone

* Corresponding author.
E-mail address: Jagoda.Crawford@ansto.gov.au (J. Crawford).

https://doi.org/10.1016/j.atmosenv.2019.03.018
Received 1 November 2018; Received in revised form 1 March 2019; Accepted 17 March 2019
Available online 20 March 2019

concentrations (Gantt et al., 2015). According to Riedel et al. (2013), the displaced Cl atoms are highly reactive and have higher rate constants for reaction with volatile organic compounds (VOC) than hydroxyl radicals (OH). Hence, the presence of Cl can reduce the VOC concentration resulting in a higher availability of OH, which is then free to contribute to additional ozone production. Keene et al. (1990) found that losses of Cl were typically associated with elevated concentrations of anthropogenic combustion products. Thus, fresh and aged sea salt aerosols can cause an increase in the aerosol concentrations over coastal urban cities, particularly as air masses pass over anthropogenic pollution sources.

Coastal recirculation can also cause an increase of air pollution in coastal locations (e.g. Levy et al., 2009; and references therein). Recirculation events are known to occur in the Sydney Basin (Barros, 2001), due to the surrounding topography. Crawford et al. (2017) found that the highest aged sea air concentrations occurred at Lucas Heights under regional recirculation conditions. Also in the Sydney Basin, using measurements at the Westmead Air Quality Station (36 km inland), Emmerson et al. (2013) found that the sea salt component accounted for around 36% of the $PM_{2.5}$ total mass, of which 64% was from fresh emissions and 36% was aged particles (bound with nitrate or sulfate). Their model also showed that sea salt particles from as far away as the Southern Ocean could influence sea salt levels at Westmead. Gimsenius (1996) during a study of fresh sea salt concentrations in the atmosphere of New South Wales, Australia, showed a decrease further inland with a concentration of 2,004 ng m^{-3} at 0.1 km from the coast, which reduced to 87 ng m^{-3} at 199.4 km from the nearest coast.

The aims of this study are to identify the extent of sea spray impact on $PM_{2.5}$ in the coastal urban environment of the Sydney Basin. In addition, we quantify the fresh sea salt component and the component that is affected by Cl loss (i.e. the aged sea spray component). We further, identify the fetch regions and Sydney locations, causing the highest chlorine depletion. This is particularly important for the Sydney Basin, as it has been found that chlorine emissions from sea salt aerosols can enhance coastal urban ozone concentrations (Knipping and Dabdub, 2003). Similar impacts are likely at other Australian coastal urban sites.

We use data from a 20-year $PM_{2.5}$ time series (Feb-1998 to Feb-2017) from two sites in Sydney, Richmond and Lucas Heights. Positive Matrix Factorisation (PMF; Paatero and Tapper, 1994) together with Radon-222 (radon) concentrations (Chambers et al., 2011) to identify source fingerprints with marine origins.

1.1. Study sites

The two study sites are located in the Sydney Basin. Lucas Heights is located near the southern end of the Sydney Basin (34°03′S, 150°59′E; 151 m above sea level; asl) at about 30 km southwest of the Sydney CBD, and 18.4 km from the nearest coast (Fig. 1). Topography of the Lucas Heights region is complex, with 150 m changes in elevation within a 1 km radius of the site, primarily associated with a river valley east of the site. Land use in the vicinity is a mixture of suburban and natural vegetation.

Richmond (33°37′S, 150°45′E) is located 51 km northwest of Sydney's Central Business District (CBD), at 24 m asl and at about 58 km from the nearest coast (Fig. 1). Land use to the east of Richmond is urban-residential while a rural zone is located to the west. Richmond is only 10 km from the foothills of the Great Dividing Range that form the western boundary of the Sydney Basin.

These two study sites were selected because of their increasing distances from the coast, enabling the progression of the sea salt aerosols to be studied. Furthermore, Radon-222 measurements were also available at both sites.

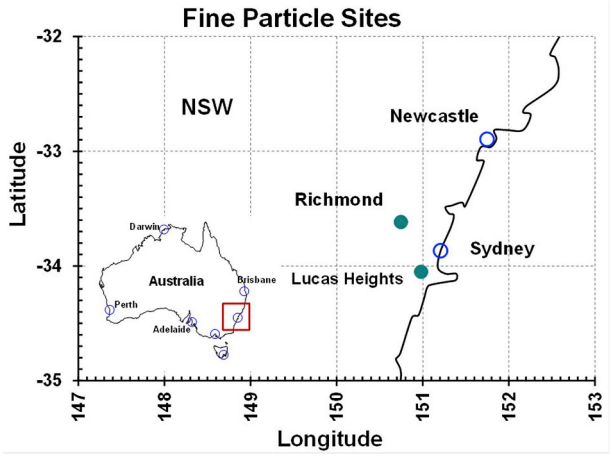

Fig. 1. Location of the Richmond and Lucas Heights sites (●) in NSW.

1.2. Aerosol sampling, elemental analysis and source fingerprint determination

Twenty-four-hour (midnight-to-midnight) continuous $PM_{2.5}$ samples have been collected twice a week (i.e. on Wednesday and Sunday) at both Richmond and Lucas Heights since 1991. A $PM_{2.5}$ sampler based on the IMPROVE cyclone system is used which samples at a flow rate of 22 L/min and a 25 mm diameter stretched Teflon filter is used for sample collection. The total $PM_{2.5}$ is measured using a Mettler Toledo MX5 microbalance under laboratory conditions of 22 °C ± 2 °C and relative humidity of 50% ± 5% with an accuracy of ± 5 μg, precision of ± 1 μg and a repeatability ± 0.8 μg. Following this accelerator-based ion beam analysis (IBA) techniques; proton induced X-ray emission (PIXE), proton induced gamma-ray emission (PIGE), proton elastic scattering analysis (PESA) and Rutherford backscattering (RBS) are used to non-destructively determine the elemental composition of the $PM_{2.5}$ filters collected (Cohen et al., 1996). From the IBA analysis the concentration of the following elements; H, N, Na, Al, Si, P, S, Cl, K, Ca, Ti, V, Cr, Mn, Fe, Co, Ni, Cu, Zn, Se, Br and Pb are obtained. The concentrations of black carbon (BC) are determined by using HeNe laser absorption techniques. The value of the absorption efficiency depends on the chemical composition of the measured aerosol particles, their size distribution, and the mixing state of the aerosol particles. A study undertaken by ANSTO to determine the most appropriate absorption coefficient for the aerosols measured at ANSTO concluded that an absorption coefficient of 7 m^2/g was most appropriate (Taha et al., 2007) for our regions.

$PM_{2.5}$ measurements between February 1998 and February 2017 were selected for use in this study, however when Radon-222 was used for the analysis the data between January 2006 to December 2009 was used, which corresponded to the period for which radon was available.

Positive matrix factorisation (PMF; Paatero and Tapper, 1994) was used to obtain the source type fingerprints (or factors). When using PMF the user needs to specify the number of source types to be determined, and typically, a number of different solutions are considered. The optimum solution is selected based on the errors of the fit (contained in the Q value) and how well the fingerprints represent known source types. When using PMF the following equation is solved:

$$X = GF + E \quad (1)$$

or

$$x_{i,j} = \sum_{k=1}^{p} g_{i,k} f_{k,j} + e_{i,j} \quad (2)$$

Where rows of $x_{i,j}$ represent the elemental composition of each samples and the columns are the separate samples. The matrix F contains the fingerprints, G is the corresponding contributions and E contains the errors of the fit. The indices i, j, k represent the number of samples, the number of element and the number of fingerprints, respectively. The optimisation process minimises the function, Q, while the resolved factor elements, of F and G, remain non-negative:

$$Q = \sum_{i=1}^{n} \sum_{j=1}^{m} \frac{e_{i,j}^2}{s_{i,j}^2} \quad (3)$$

where $s_{i,j}$ is a specified error of the form (Cohen et al., 2010):

$$s_{i,j} = MDL_{i,j} + Error_{i,j} \max(|x_{i,j}|, |y_{i,j}|) \quad (4)$$

where $MDL_{i,j}$ is the minimum detectable limit, $Error_{i,j}$ is the statistical error, and $y_{i,j}$ is the fitted value i.e. Y = GF.

For $PM_{2.5}$ samples in the Sydney Basin, seven or eight source types are normally sufficient. Here between five and eight fingerprints were examined and it was found that the total $PM_{2.5}$ mass was consistently best explained by seven fingerprints. The fingerprinting method and composition of each source fingerprint is detailed in (Crawford et al., 2016 and 2018b), for Lucas Heights and Richmond, respectively.

The identified source fingerprints (at Richmond; Lucas Heights) were vehicle exhaust (*Autos*; 18%; 26.3%), secondary sulfate (*2ndryS*; 24%; 23.7%), aged sea air mixed with industrial sources (*IndSaged*; 16%; 20.6%), smoke from domestic heating or bush fires (*Smoke*; 31%; 13.7%), fresh sea salt (*Sea*; 4.8%; 10.9%), soil dust (*Soil*; 4.1%; 3.7%) and other industrial releases (2.1%; 1.1%).

The elemental composition of the source fingerprints are presented in Supplementary Figs. S1 and S2, for brevity, only the *Sea* and *IndSaged* fingerprints will be reproduced here in the results and discussion section 2.

1.3. Atmospheric Radon-222 measurements

Radon-222 (radon) is a naturally occurring radioactive noble gas emitted from soils and rocks. The radon source term over land is well constrained (16–26 mBq m^{-2} s^{-1}; Schery and Wasiolek, 1998; Goto et al., 2008) while over the ocean the source term is 2–3 orders of magnitude lower. As a result radon is widely used as a tracer of recent terrestrial influence (2–3 weeks) on air masses in atmospheric transport studies (e.g. Balkanski et al., 1992; Zahorowski et al., 2004; Zhang et al., 2008; Chambers et al., 2009, 2014; 2016; Koffi et al., 2016).

Radon measurements at Lucas Heights and Richmond began in 2006; and measurements at Lucas Heights are ongoing. A description of the Lucas Heights radon detector is given in Chambers et al. (2011). In this study we use radon, when available, to identify the degree of terrestrial influence on air masses. 24-hour averaged radon measurements were used in the analysis, corresponding to the 24-hr $PM_{2.5}$ measurement window.

1.4. Back trajectory analysis and concentration weighted trajectories

For each day on which $PM_{2.5}$ samples were available, 24 back trajectories were generated (one for each hour corresponding to the duration of sample collection). The back trajectories were generated using HYSPLIT (HYbrid Single-Particle Lagrangian Integrated Trajectory; Draxler et al., 2016; Stein et al., 2015), which requires meteorological datasets. The 1° by 1° meteorological datasets generated by the global data assimilation system (GDAS) model which is run by the National Weather Service's (NWS) National Centre for Environmental Prediction (NCEP; available at ftp://arlftp.arlhq.noaa.gov/archives/gdas1) were downloaded and used. However, these datasets are available from 2000 onwards; hence, back trajectories were generated for this period only.

When generating back trajectories a number of options need to be specified, back trajectory starting height at the sampling location (i.e. the altitude at which the air mass arrived at the sampling site), the length in time for which the back trajectories are tracked and how often the 3D locations of the back trajectories (latitude, longitude and altitude) are to be recorded. Here the back trajectories were tracked for 5 days and their location was recorded every 30 min. Back trajectories were calculated from two starting elevations (300 and 500m a.s.l.), but very little difference in the results was obtained. We therefore chose to use the results from the 300m starting heights, since this elevation would be more representative of a larger number of boundary layer events at night (for each 24 h period) when mixing near the surface is not as deep. Given that there are changes in terrain elevation in the vicinity of the Lucas Heights site in excess of 100m, we thought it best not to use a trajectory starting height any lower than 300m.

Along the 5-day back trajectories, averages of selected variables available from the meteorological data files were calculated, including: altitude of the back trajectory, rainfall amount, relative humidity, solar radiation, wind speed, and the time that the air mass spent over land. Averages were calculated at the air mass' altitude, not at surface level.

Back trajectory density maps were generated for the region using a 0.1° by 0.1° resolution grid. If a back trajectory passed over a grid cell a counter was incremented. Since the atmospheric boundary layer over land can reach heights of 2,300 m (Anthes, 1978), if the back trajectory height was above 2,000 m at a given location the cell counter was not incremented.

The concentration weighted trajectory method (CWT; Hsu et al., 2003) was used to determine regions that potentially contributed to high concentrations at the measurement site. In the CWT method, each grid cell gets a weighted concentration obtained by averaging sample concentrations corresponding to trajectories that crossed that grid cell:

$$C_{ij} = \frac{1}{\sum_{l=1}^{M} \tau_{ijl}} \sum_{l=1}^{M} C_l \tau_{ijl}$$

where, C_{ij} is the average weighted concentration in the grid cell (i,j), τ_{ijl} is an indicator equal to 1 if a trajectory has passed through grid cell (i,j), C_l is the measured concentration of sample l, and M is the total number of samples.

2. Results and discussion

Elemental compositions for the full set of source fingerprints are presented in the supplementary information and have been discussed in detail in Crawford et al. (2016 and 2018b, for Lucas Heights and Richmond, respectively). In this study, we were mainly concerned with identifying anthropogenic sources contributing to the aged sea salt fingerprint (*IndSaged*), although we present both the fresh *Sea* and *IndSaged* fingerprints for completeness (Fig. 2).

The explained variation of each element by each fingerprint (Paatero, 2004) is presented in Tables S1 and S2 of the supplementary information. The variation of the fresh sea salt fingerprint explains a large proportion of the variation in Cl (97% and 99% at Lucas Heights and Richmond, respectively), whereas the variation in the *IndSaged* fingerprint explains a large proportion of the variation of Na (56% and 85% at Lucas Heights and Richmond, respectively). The fresh sea salt and *IndSaged* fingerprint accounted for 20% of the variation in K at Lucas Heights, whereas at Richmond 22% of the variation in K was accounted for by the *IndSaged* fingerprint. At Lucas Heights, 1.1% of the measured K was allocated to the fresh sea salt fingerprint, 6.3% to the *IndSaged* fingerprint and 87.6% to the *Smoke* fingerprint. At Richmond, K was absent from the fresh sea salt fingerprint, however, an uncertainty in K was recorded in the fingerprints (Figs. S1 and S2 in the supplementary information). This indicates some loss of K from the fresh sea salt fingerprint with distance from the coast.

At Lucas Height 2.5% of the nitrogen was allocated to the fresh sea salt fingerprint. No nitrogen was present in the *IndSaged* fingerprint at

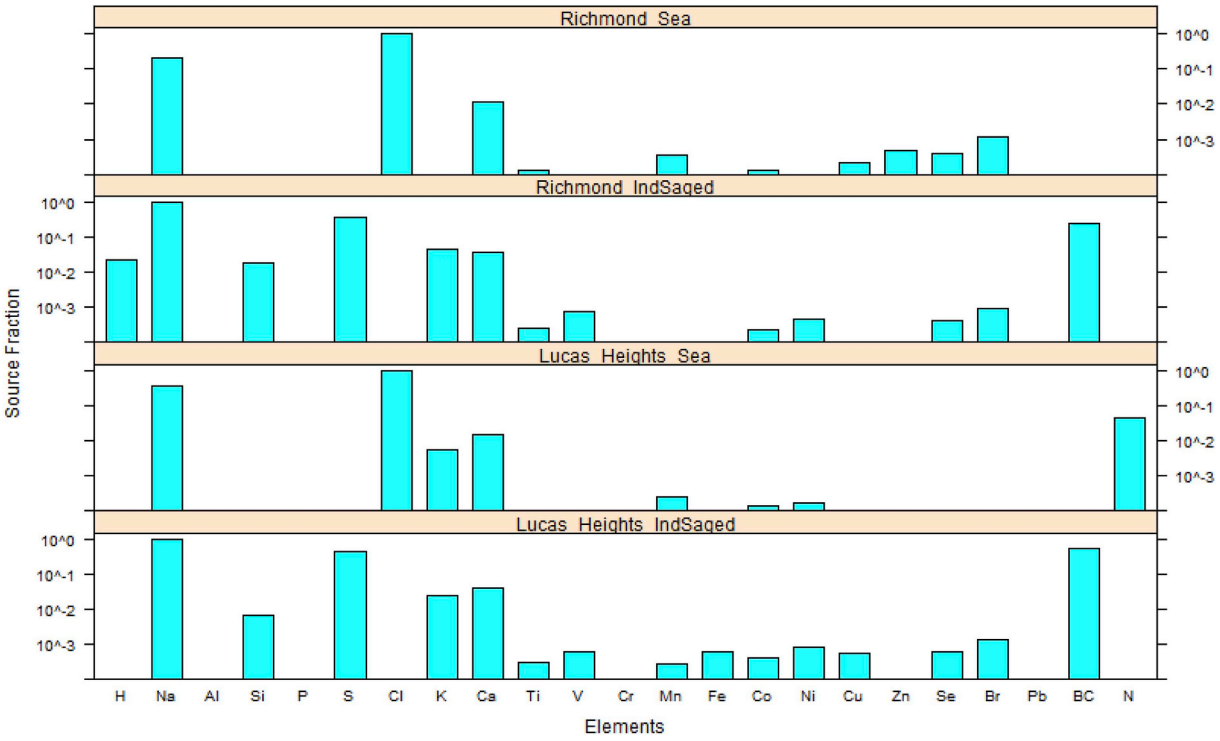

Fig. 2. Elemental composition of the fresh *Sea* and *IndSaged* fingerprints at Richmond and Lucas Heights.

either site, although the PMF reconstruction indicated that this was not absolute zero, as an uncertainty was reported in the fingerprints; see Supplementary Figs. S1 and S2. Pio and Lopes (1998) found that reactions with sulfur-containing pre-cursors were responsible for greater loss of chlorine from fine particles, whereas nitrogen-containing pre-cursors were more responsible for chlorine loss in the coarser particles. However, Bondy et al. (2017) reported that, during inland transport of sea salt, sulfate-containing particles were present in the 0.5–5 μm particle range and particles containing nitrate were mostly in particles above 1 μm. An explanation of the mechanisms of formation is presented in Bondy et al. (2017; and references therein): the accumulation of sulfate in sea spray aerosol by reaction with SO_2 is diffusion limited. Thus it occurs most readily in $PM_{2.5}$ particularly accumulation mode particles. "Additionally, sulfate may accumulate in small particles because H_2SO_4, acid formed from the aqueous-phase or gas-phase oxidation of SO_2 in deliquesced particles and droplets, dissociates instantly to HSO_4^-, H^+, and SO_4^- and stays in the particle phase after uptake or formation, as opposed to the higher vapour pressure HNO_3." Deposition of particles may also play role in the depletion of nitrogen containing aerosols with transport from the coast to inland sites, as the larger particles would deposit earlier. Giorgi (1988) shows an increase in deposition velocities for particles with diameter greater than 0.1 μm.

Average concentrations of fresh and aged sea spray at Cape Grim are also presented below for comparison; a full description of the source fingerprints at Cape Grim has been presented in Crawford et al. (2018a). Cape Grim is a coastal station located on the north-western tip of Tasmania and, due to its location, is directly affected by fresh oceanic air for a large proportion of the year.

At both, Richmond and Lucas Heights, sulfur was absent from the fresh sea salt fingerprint, although an uncertainty is reported by the PMF process (see Supplementary Figs. S1 and S2). However, at Cape Grim 10% of the sulfur was allocated to the fresh sea salt fingerprint. Assuming that the composition of oceanic air masses near Cape Grim and off the Sydney coast are the same, this would indicate loss of sulfur from the fresh sea salt fingerprint over land.

The concentrations of fresh *Sea* and *IndSaged* sources for the three sites, which have increasing distances from their respective coasts, are presented in Table 1. A decrease in the fresh *Sea* salt concentration as well as its fractional contribution to the total $PM_{2.5}$ was seen further inland. The *IndSaged* component shows higher concentrations at 18 km from the coast than that at 58 km from the coast (about a 20% decrease over 39 km). The location of Cape Grim is such that little impact is seen from anthropogenic releases from the Australian mainland for a large proportion of the year, hence the low *IndSaged* component. The direct influence of the Southern Ocean on this site is responsible for the high fresh *Sea* salt component.

Table 1
Average concentrations (μg m^{-3}) and fraction of total $PM_{2.5}$ for fresh and aged sea salt at sites located 0.1, 18, and 58 km from coast.

Source	Cape Grim	Cape Grim	Lucas Heights	Richmond	Richmond
	(1998–2016)	(2001–2009)	(2001–2009)	(1998–2017)	(2001–2009)
Distance to coast (km)	0.1	0.1	18	58	58
Sea μg/m^3	3.26 ± 0.05	3.16 ± 0.05	0.47 ± 0.02	0.26 ± 0.01	0.23 ± 0.01
IndSAged μg/m^3	0.61 ± 0.01	0.65 ± 0.01	1.08 ± 0.03	0.87 ± 0.02	0.83 ± 0.02
Percentage of total $PM_{2.5}$					
% total marine aerosols	69	69	32	21	18
Fresh	57	56	11	4.8	4
Aged	12	13	21	16	14

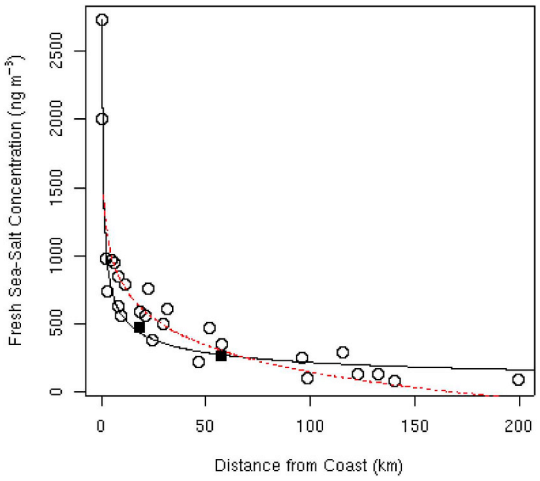

Fig. 3. Average fresh sea salt concentration with distance from the nearest coast (adapted from Gimsenius, 1996). The black line shows the power fit ($1434x^{-0.411}$) and the red dashed line is the ln fit ($-281.9\ln(x) + 1445$). The solid squares are the results from this study. (For interpretation of the references to colour in this figure legend, the reader is referred to the Web version of this article.)

Gustafsson and Franzén (2000) found that the decreasing concentration of fresh sea salt with distance inland could be approximated using a power function ($c/c_s = 2.29D^{-0.46}$; where c was the sea salt concentration in air at a downwind distance D from the coast and c_s was the sea salt concentration at the coast). In New South Wales, the trend in fresh sea salt with distance from the coast (using annual average data for 1993 from Gimsenius, 1996; where data for 26 locations was available) is presented in Fig. 3. The power function fit had an exponent of −0.41, which is close to that of Gustafsson and Franzén (2000). A better R^2 value (0.89 as opposed to 0.78 for the power function) was obtained if the natural log functions were used in the fitting process. Although the two data points from this study plot closer to the curve generated using the power function fit than to the data presented in Gimsenius (1996).

2.1. Aged sea salt composition

Foltescu et al. (1996) pointed out that sodium is a conservative element and that the Cl/Na ratio is a good measure of chlorine depletion. In this study, the Cl/Na ratios at Lucas Heights and Richmond were 0.72 and 0.87, respectively in comparison to 1.54 for fresh sea salt. This indicates a general loss of chlorine away from the coast, but a larger chlorine loss at Lucas Heights compared with Richmond despite the latter site being further from the coast. This may be connected with the generally higher *IndSaged* concentrations seen at Lucas Heights compared to Richmond (Table 1). Hallal et al. (2013) analysed elemental composition of aerosol particles in the greater Sydney region in 2002–2003, and found excess sodium, which they concluded was in part as a result of chlorine depletion. They found a reduction in the Cl/Na ratio with distance from the coast, indicating less fresh sea salt further inland.

McInnes et al. (1994), in studying the chloride depletion in individual sea salt particles, found that the elemental ratios of Ca/Na, Mg/Na, and K/Na remain fairly constant between particles of various sizes for more than 85% of the particles examined. From Marine Science (2018), in seawater the following ratios hold: Ca/Na = 0.039 and K/Na = 0.036. For the *IndSaged* fingerprint, at Richmond, the Ca/Na and K/Na ratios were both 0.037; at Lucas Heights, the corresponding ratios

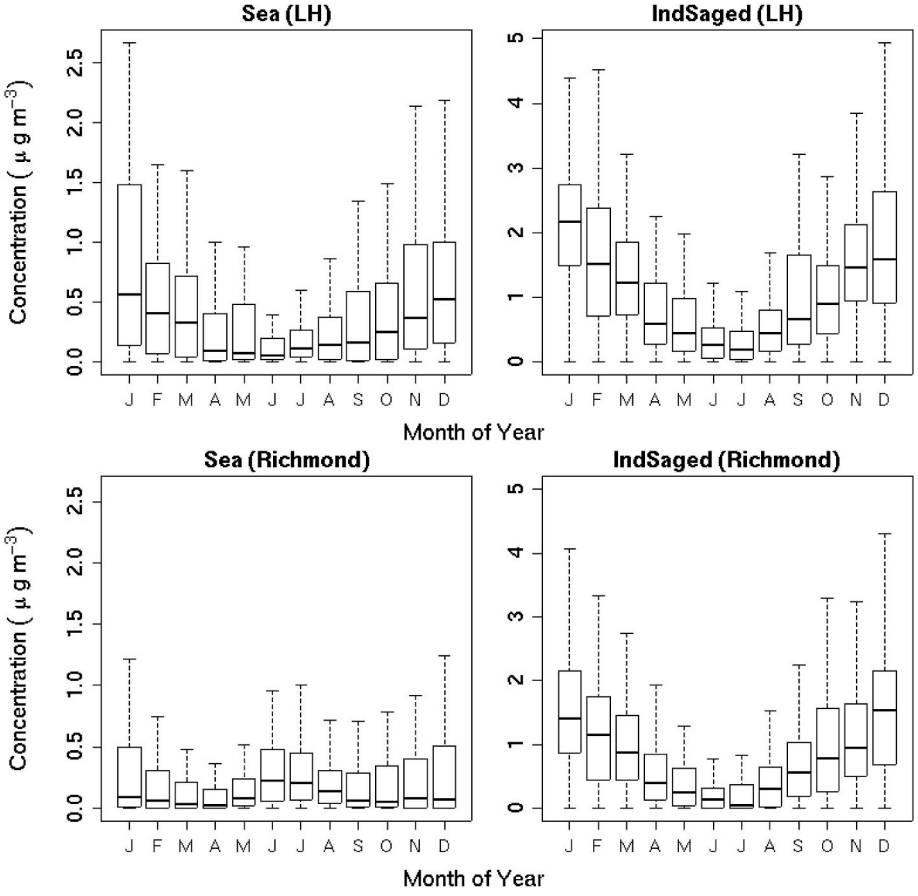

Fig. 4. Fresh *Sea* salt and *IndSaged* fingerprint concentration at Lucas Heights (LH) and Richmond by month of year, for the study period.

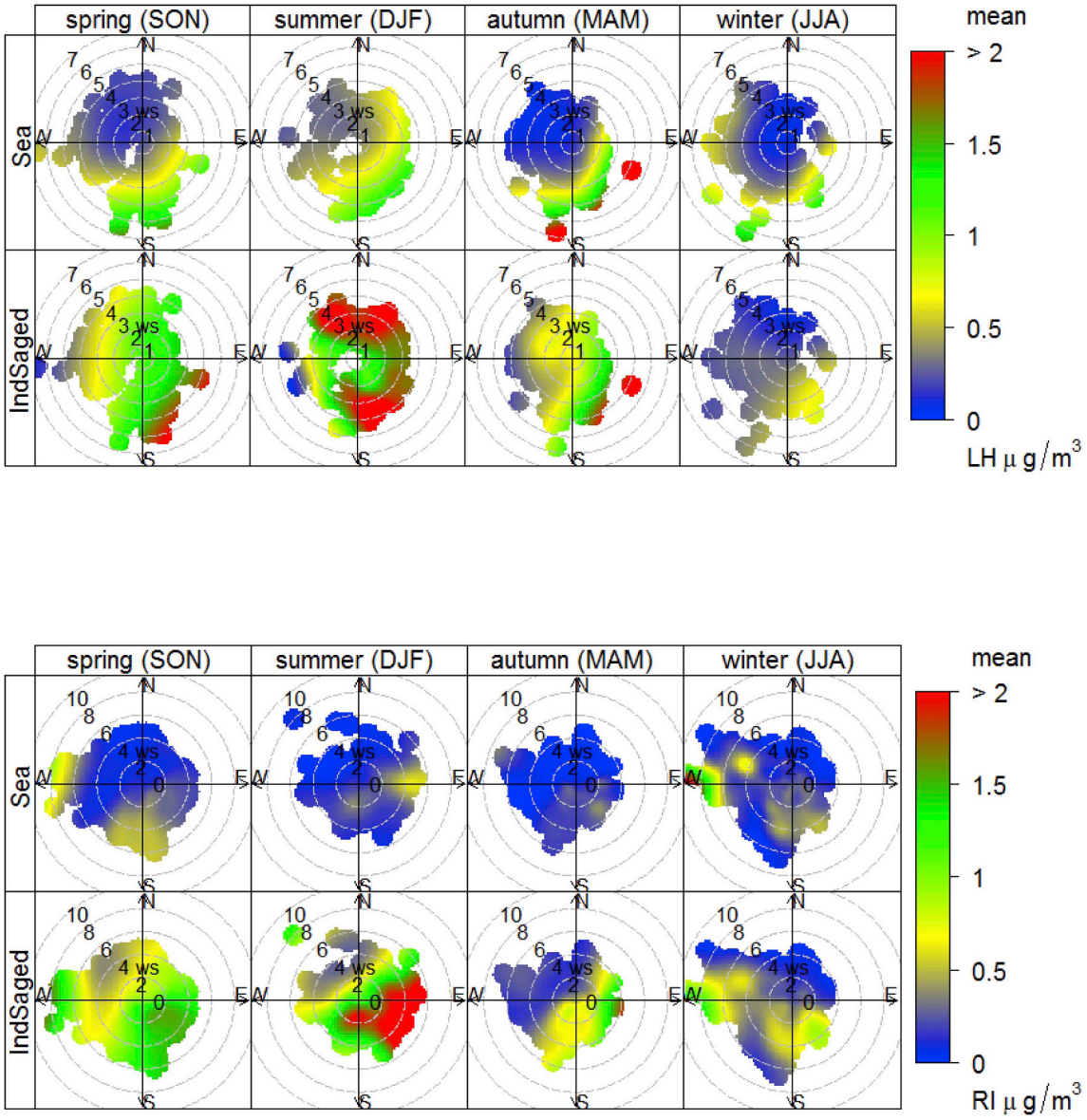

Fig. 5. Concentrations of fresh sea salt and *IndSaged*, by season and by sector, at Lucas Heights (LH) and Richmond (RI). The plot was generated using the R package openair (Carslaw and Ropkins, 2012).

were 0.038 and 0.026, respectively. The lower ratio of K/Na at Lucas heights indicates some K loss (as the Ca/Na ratio was close to 0.039). Further, in the *IndSaged* fingerprint, the S/Na ratio at Richmond was 0.39 and at Lucas Heights it was 0.43 (compared to 0.06 for seawater) and about 26% of the measured sulfur was allocated to the *IndSaged* fingerprint. Mg concentrations were not available through the IBA, hence could not be considered here.

In this study, higher *IndSaged* concentrations were measured at Lucas Heights. However, from Table 1, the ratio of the *IndSaged* concentration to the fresh sea salt (*Sea*) concentration was 2.3 at Lucas Heights and 3.3 at Richmond (for 1998 to 2017, and 3.6 for 2001 to 2009; corresponding to the time span for Lucas Heights), indicating overall a larger conversion from fresh to aged sea salt further inland. The elemental ratios in the *IndSaged* fingerprint indicate more Cl and K loss at Lucas Heights than at Richmond and alternatively a higher S composition at Lucas Heights than at Richmond. Possible contribution to this could be the meteorology and/or differences in the anthropogenic sources over which the air masses have travelled before sampling at the sites (as seen and further investigated in section 2.4).

2.2. Seasonal concentrations and fetch regions

In general, atmospheric concentrations of the sea salt aerosol exhibit a seasonal variation, with differences in winter and summer estimates a factor of 2–3, mainly due to the seasonal variations of the wind speed (Erickson et al., 1986) and direction.

The seasonal variation in concentration of fresh *Sea* salt and *IndSaged* is presented in Fig. 4. The corresponding polar concentration plots are presented in Fig. 5. Higher wind speeds were seen in summer and more often from the east side (the direction of the closest coast), corresponding to higher summer concentrations of fresh *Sea* salt, at Lucas Heights and *IndSaged*, at both sites (Fig. 4). That is, in Sydney in

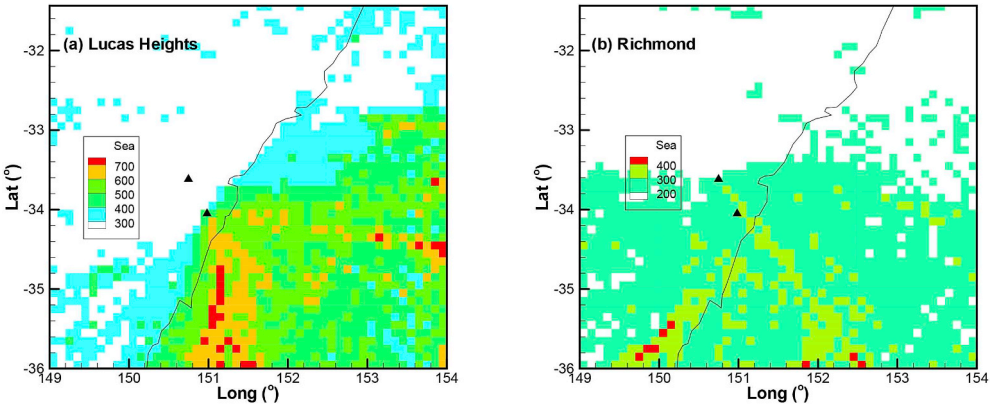

Fig. 6. CWT of Fresh Sea salt at (a) Lucas Heights and (b) Richmond. Location of Lucas Heights and Richmond marked with a black triangle.

summer months a large proportion of the fetch is from the ocean whereas in winter months a higher proportion of the fetch is from continental Australia (western side). In addition, the variability in concentrations would be affected by the wind speed, as can be seen in Fig. 5 where the higher concentrations occur when the wind speeds are higher. In winter, there is a small peak of fresh *Sea* salt at Richmond, and correspondingly a low concentration of *IndSaged*, which could be an indication of a lower conversion rate from fresh to aged sea salt.

The impact of the fetch region is particularly obvious in the summer polar concentration plots of the *IndSaged* fingerprint in Fig. 5. Due to their locations, the Lucas Heights site receives higher concentrations from the north and southeast. This is the result of air mass passage over populated regions before arriving to the Lucas Heights measuring location. On the other hand, Richmond receives higher concentrations from the south-east in the direction of the major population and little from the north in the direction of natural vegetation.

2.3. Concentration weighted trajectory (CWT) maps

Concentration Weighted Trajectory (CWT) maps of fresh *Sea* salt and *IndSaged* are presented in Fig. 6 and Fig. 7, respectively. At both sites, the highest concentrations of fresh *Sea* salt were reported when fetch was from the south-east sector, corresponding also to the higher wind speeds (Fig. 5). At Richmond, the highest concentrations of *IndSaged* occur when the air masses were arriving from the south-east quadrant; however, at Lucas Heights high concentrations of *IndSaged* were also recorded when the air masses were arriving from the north-east quadrant under high wind speed in summer (Fig. 5). This is in the relative location of the Sydney central business district (CBD). Furthermore, for each sampling day the time spent overland by an air mass before arriving at the sampling site was estimated. The highest concentrations of fresh *Sea* salt occurred within 1 h at Lucas Heights and about 2 h at Richmond. On the other hand, the highest concentrations of *IndSaged* occurred between 4 and 6 h at Lucas Heights and 8 h at Richmond (presented in Supplementary Figs. S3 and S4). This is examined further in the following section.

2.4. Relationship between radon and aerosols concentrations

Radon is a good indicator of the degree of terrestrial influence on an air mass – the higher the radon concentration the more terrestrially influenced the air mass. The results in Fig. 8 confirm that the precursors to *IndSaged* originate from the ocean as the concentrations decrease with increasing radon, at both sites. The concentrations in the summer months are higher, as presented by the green stars in Fig. 8.

To examine the variations in fresh *Sea* salt and *IndSaged* concentrations under low land fetch conditions, the samples with the bottom 10% of radon were identified (38 samples for Richmond and 29 samples for Lucas Heights), from which four groups were formed; top and bottom 15% of fresh sea salt and top and bottom 15% of aged sea salt (5 and 6 samples in each group at Lucas Heights and Richmond, respectively). Twenty-four back trajectories were generated for each sample in each group (i.e. one corresponding to each hour of the $PM_{2.5}$ sampling day) and average values of a number of variables were

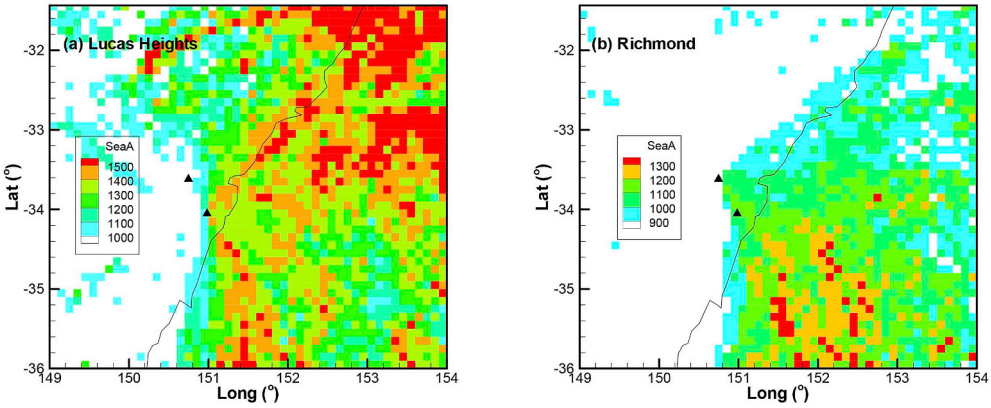

Fig. 7. CWT of Aged Sea Air at (a) Lucas Heights and (b) Richmond. Location of Lucas Heights and Richmond marked with a black triangle.

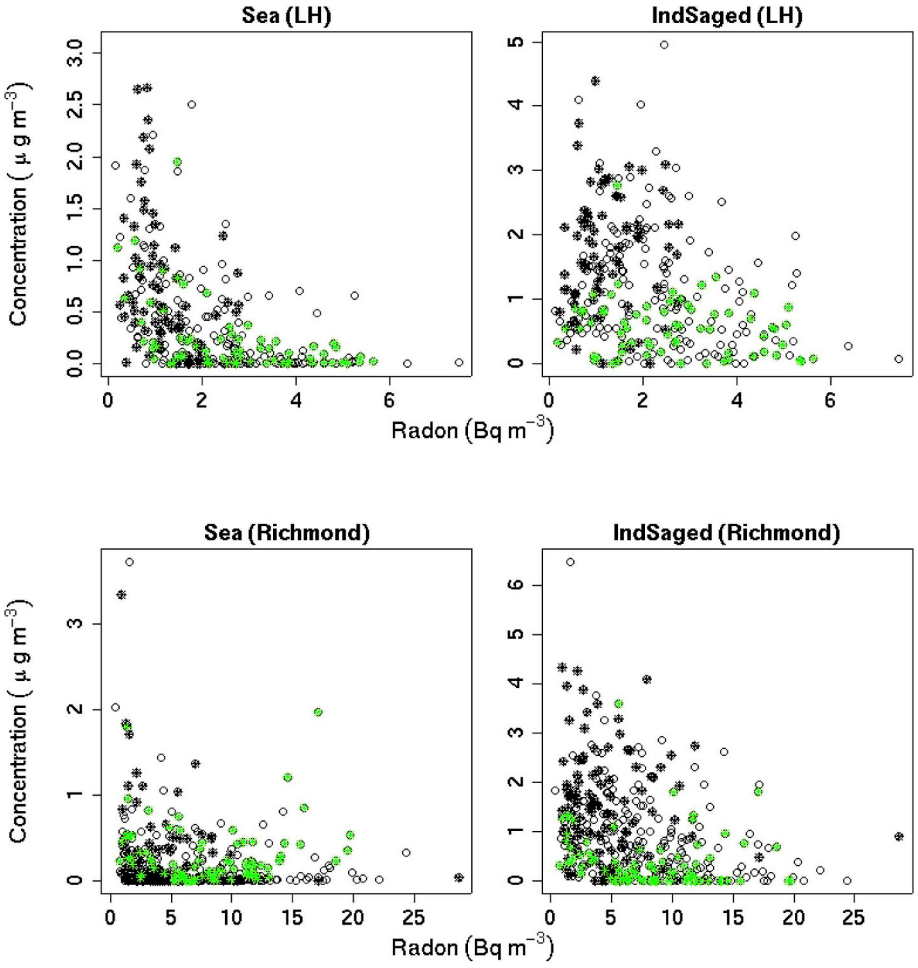

Fig. 8. Fresh *Sea* salt and *IndSaged* concentrations against radon at Lucas Heights and Richmond. Black and green stars represent summer and winter data, respectively. (For interpretation of the references to colour in this figure legend, the reader is referred to the Web version of this article.)

calculated (Table 2) and the corresponding back trajectory density maps are presented in Fig. 9 and Fig. 10, for Lucas Heights and Richmond, respectively.

Both at Lucas Heights and at Richmond, the difference between the two groups of fresh sea salt was that for periods when lower concentrations of fresh sea salt was measured; the air masses were arriving from the south-east (Figs. 9a and 10a) at a higher altitude (Table 2) and the air masses had spent less time overland and were mostly arriving directly from the east coast under higher wind speed. Higher wind speed would have resulted in more sea salt aerosol formation (Prijith et al., 2014) and the lower travel time would have resulted in lower loss due to either chemical reactions or deposition.

The difference between the two groups of *IndSaged* samples was that for periods when higher *IndSaged* concentrations were measured, the majority of air masses had passed over the populated urban Sydney Basin. These events occurred between October and January (Figs. 8d

Table 2
Average values of selected variables, for each of the four different groups (for both Lucas Heights and Richmond). The first five columns contain the average values of the parameter along the back trajectory.

	Altitude (m)	Rainfall (mm/h)	Relative Humidity (%)	Solar Radiation (watts/m^2)	Wind Speed (km/h)	Time over Land (h)	Aged Sea Conc. (ng/m^3)	Fresh Sea Conc. (ng/m^3)	Average Radon (Bq/m^3)
Lucas Heights									
Low Sea	170	0	72.5	232	6.5	3.3	1378	206	536
High Sea	154	0.2	69.2	241	10.3	2.4	17078	1899	431
Low *IndSaged*	227	0	74.7	157	8.7	1.3	3388	710	378
High *IndSaged*	114	0	71.9	339	7	3.1	3069	1250	562
Richmond									
Low Sea	415	0.1	77.1	262	8.8	9.4	1239	14	1343
High Sea	344	0.1	73.8	207	14.4	6.7	2749	2093	1130
Low *IndSaged*	234	0.3	77.2	137	11	11.2	269	139	1304
High *IndSaged*	380	0.1	73.7	279	12.1	5.6	2959	1353	1226

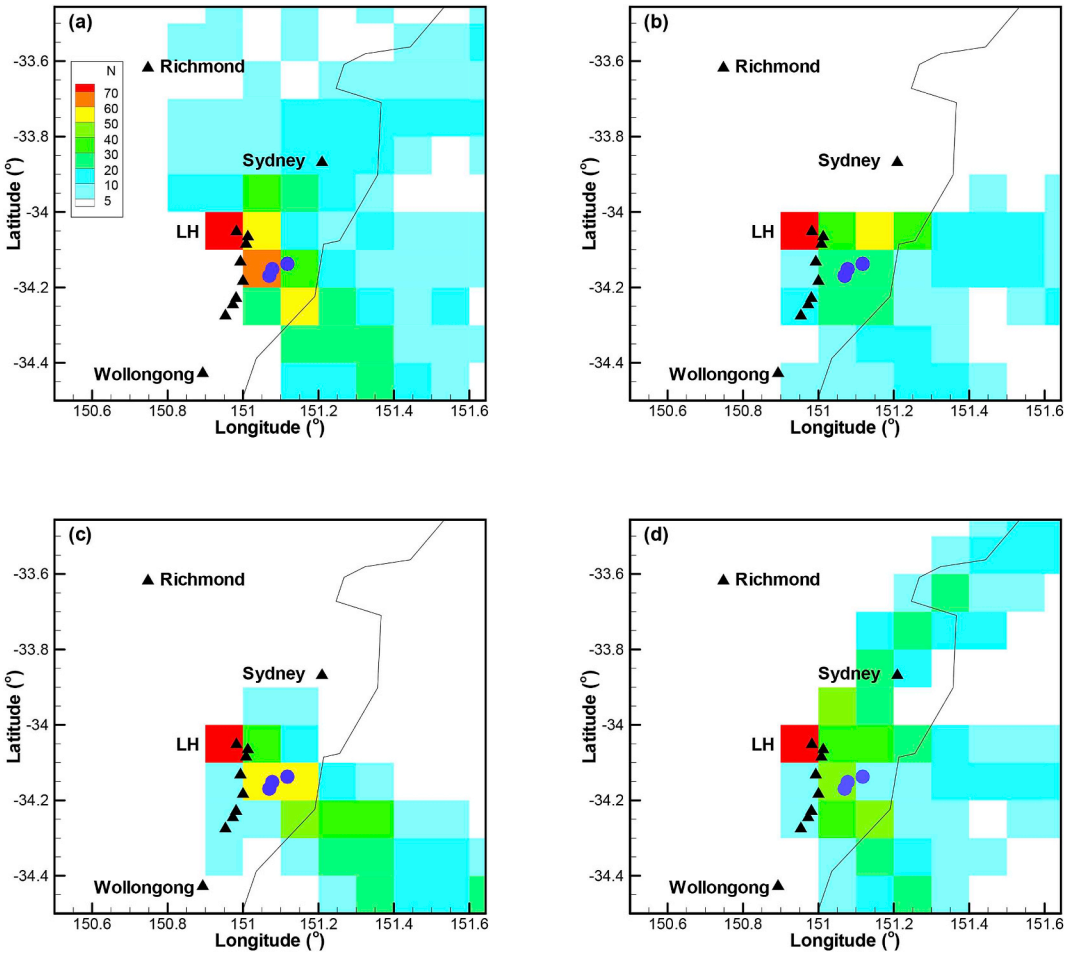

Fig. 9. Back trajectory density plots at Lucas Heights (a) Low *Sea*, (b) High *Sea*, (c) Low *IndSaged*, (d) High *IndSaged*. Black triangles mark suburbs and the blue circles are reserves. (For interpretation of the references to colour in this figure legend, the reader is referred to the Web version of this article.)

and 10d; also corresponding to periods of highest solar radiation, thus increased reaction rates, Keene et al., 1990). For Lucas Heights, the fetch region was to the northeast in the direction of the Sydney CBD. In addition, for Lucas Heights some back trajectories had also arrived from the south east, in the direction of nearby towns (Heathcote and Waterfall) and the Princes Highway (the main road linking southern urban regions to Sydney, with an average daily vehicle count of about 24,300; Road and Maritime Services, 2018). In addition, this is also in the direction of Wollongong with significant industry including steelworks. In the case of Richmond, the fetch region was south-east, indicating that vehicle exhausts and releases from small industries (e.g. metal and coal product manufacturing, bricks and pavers production in Schofields) in this region had an impact on the *IndSaged* concentrations.

On the other hand, low *IndSaged* occurred when a large proportion of air masses were arriving from the south at Richmond and south-east at Lucas Heights. At Lucas Heights the majority of air masses had passed over the Royal National Park reserves directly south-east of the site (Fig. 9c; yellow region and blue circle markers). The air masses were traveling at a higher altitude under low solar radiation conditions (Table 2). At Richmond the air masses had passed over the less polluted regions south of Richmond on the outskirts on the Sydney Basin (Fig. 10c). No major industry is located in this sparsely populated region. In addition low solar radiation conditions prevailed and the air masses had spent more time over land, i.e. further removed from the oceanic source region (Table 2).

3. Conclusions

The concentrations of fresh and aged sea salt (or *IndSaged*), were determined from PMF analysis of our long-term elemental data set spanning the period 1998 to 2017 at two sites in the Sydney basin with varying distance from the nearest coast. At Lucas Heights, located at 18.4 km from the nearest coast, the average concentrations of fresh and aged sea spray were 0.47 ± 0.02 and 1.08 ± 0.03 μg/m^3, respectively. At Richmond, located at 58 km from the coast, the average concentrations of fresh and aged sea spray were 0.26 ± 0.01 and 0.87 ± 0.02 μg/m^3, respectively. At Lucas heights, fresh sea spray contributed to 11% of the $PM_{2.5}$ and aged sea spray contributes to 21% of $PM_{2.5}$. At Richmond, fresh and aged sea salt contributes to 4.8 and 16%, respectively.

Generally, higher *IndSaged* concentrations were found at Lucas Heights compared to Richmond, despite the latter site being further from the coast. This was accompanied with a greater loss of chlorine and potassium from the sea salt sampled at Lucas Heights, and higher sulfur levels. Back trajectory and radon analyses indicated that these effects are as a result of different local fetch regions for the sea air sampled at the two sites, with sea air arriving at Lucas Heights in summer passing more frequently over the Sydney CBD and industrial areas to the south.

The difference between two groups, of low and high concentrations, of *IndSaged* samples was that for periods when higher *IndSaged*

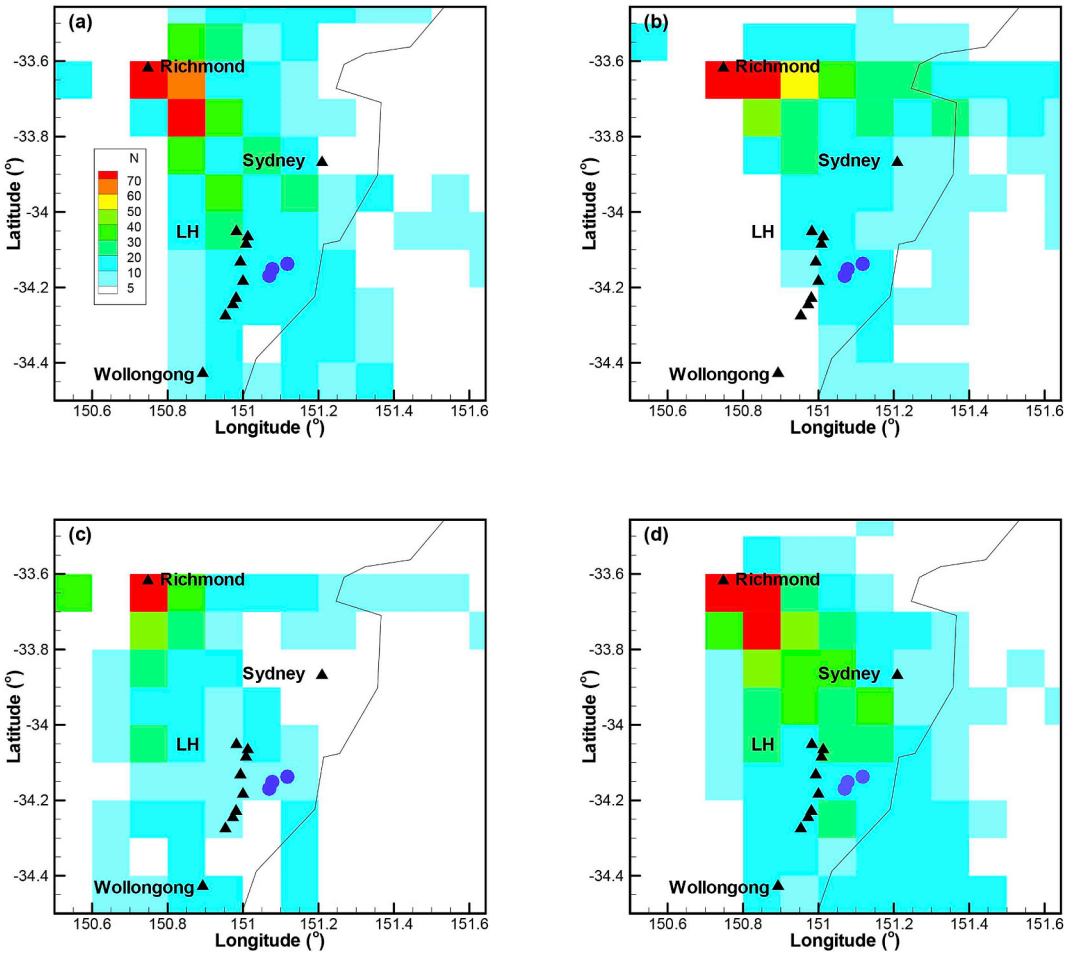

Fig. 10. Back trajectory density plots at Richmond (a) Low *Sea*, (b) High *Sea*, (c) Low *IndSaged*, (d) High *IndSaged*. Black triangles mark suburbs and the blue circles are reserves. (For interpretation of the references to colour in this figure legend, the reader is referred to the Web version of this article.)

concentrations were measured, the majority of air masses had passed over the populated urban Sydney Basin, indicating that more chlorine loss occurred over the urban regions. This is particularly important, as it has been found that chlorine emissions from sea salt aerosols can enhance coastal urban ozone concentrations (Knipping and Dabdub, 2003). Similar impacts are likely at other coastal urban sites, indicating that the geographic locations of some industries should be reconsidered.

Acknowledgements

The authors would like to acknowledge National Collaborative Research Infrastructure Strategies (NCRIS) for funding of the accelerators and Centre for Accelerator Science staff for access to their ion beam analysis facilities. The NOAA Air Resources Laboratory (ARL) made available the HYSPLIT transport and dispersion model. We also acknowledge the staff and students of the University of Western Sydney for the weekly filter changes of cyclone sampling unit during this study.

Appendix A. Supplementary data

Supplementary data to this article can be found online at https://doi.org/10.1016/j.atmosenv.2019.03.018.

References

Adachi, K., Buseck, P.R., 2015. Changes in shape and composition of sea-salt particles upon aging in an urban atmosphere. Atmos. Environ. 100, 1–9.

Anthes, R.A., 1978. The height of the planetary boundary layer and the production of circulation in a Sea breeze model. J. Atmos. Sci. 35, 1231–1239.

Balkanski, Y.J., Jacob, D.J., Arimoto, R., Kritz, M.A., 1992. Distribution of ^{222}Rn over the North Pacific: implications for continental influences. J. Atmos. Chem. 14, 353–374.

Barros, J.A., 2001. Sydney Basin: Air Toxic Emissions and Health Update. http://www.areco.org/SYDNEY%20BASIN.pdf.

Bondy, A.L., Wang, B., Laskin, A., Craig, R.L., Nhliziyo, M.V., Bertman, S.B., Pratt, K.A., Shepson, P.B., Ault, A.P., 2017. Inland sea spray aerosol transport and incomplete chloride depletion: varying degrees of reactive processing observed during SOAS. Environ. Sci. Technol. 51, 9533–9542.

Carslaw, D.C., Ropkins, K., 2012. Openair — an R package for air quality data analysis. Environ. Model. Soft. 27–28, 52–61.

Chambers, S., Zahorowski, W., Matsumoto, K., Uematsu, M., 2009. Seasonal variability of radon-derived fetch regions for Sado Island, Japan, based on three years of observations: 2002-2004. Atmos. Environ. 43, 271–279. https://doi.org/10.1016/j.atmosenv.2008.09.075.

Chambers, S., Williams, A.G., Zahorowski, W., Griffiths, A., Crawford, J., 2011. Separating remote fetch and local mixing influences on vertical radon measurements in the lower atmosphere. Tellus B 63, 843–859. https://doi.org/10.1111/j.1600-0889.2011.00565.x.

Chambers, S.D., Hong, S.-B., Williams, A.G., Crawford, J., Griffiths, A.D., Park, S.-J., 2014. Characterising terrestrial influences on Antarctic air masses using Radon-222 measurements at King George Island. Atmos. Chem. Phys. 14, 9903–9916. https://doi.org/10.5194/acp-14-9903-2014. www.atmos-chem-phys.net/14/9903/2014/.

Chambers, S.D., Podstawczyńska, A., Williams, A.G., Pawlak, W., 2016. Characterising the influence of atmospheric mixng state on Urban heat Island Intensity using Radon-222. Atmos. Environ. 147, 355–368.

Cohen, D.D., Bailey, G.M., Kondepudi, R., 1996. Elemental analysis by PIXE and other IBA techniques and their application to source fingerprinting of atmospheric fine particle pollution. Nucl. Instrum. Methods 109, 218–226.

Cohen, D.D., Crawford, J., Stelcer, E., Bac, V.T., 2010. Characterisation and source apportionment of fine particulate sources at Hanoi from 2001 to 2008. Atmos. Environ. 44, 320–328.

Crawford, J., Chambers, S., Cohen, D., Williams, A., Griffiths, A., Stelcer, E., Dyer, L., 2016. Impact of meteorology on fine aerosols at Lucas heights, Australia, atmos. Environ. Times 145, 135–146.

Crawford, J., Cohen, D.D., Griffiths, A.D., Chambers, S.D., Williams, A.G., Stelcer, E., 2017. Impact of atmospheric flow conditions on fine aerosols in Sydney, Australia. Aerosol Air Qual. Res. 17, 1746–1759.
Crawford, J., Cohen, D.D., Atanacio, A., 2018a. Long Term fine aerosols at the Cape Grim global baseline station: 1998 to 2016. Atmos. Environ. 166, 34–46.
Crawford, J., Cohen, D.D., Atanacio, A., 2018b. The impact of closure of coal-fired power stations on aerosol concentrations in the Sydney Basin. Atmos. Pollut. Res. 9, 1167–1176.
Draxler, R., Stunder, B., Rolph, G., Stein, A., Taylor, A., 2016. Hysplit4 User's guide version 4 - last revision: february 2016. https://www.arl.noaa.gov/documents/reports/hysplit_user_guide.pdf.
Emmerson, K., Cope, M., Galbally, I., Keywood, M., Selleck, P., 2013. Aged sea salt aerosol in the urban Sydney environment: a cause for concern? In: 21st International Clean Air and Environment Conference, Sydney, 7-11 September.
Erickson, D.J., Merrill, J.T., Duce, R.A., 1986. Seasonal Estimates of global atmospheric sea-salt distribution. J. Geophys. Res. 91, 1067–1072.
Feng, L., Shen, H., Zhu, Y., Gao, H., Yao, X., 2017. Insight into generation and evolution of sea-salt aerosols from field measurements in diversified marine and coastal atmospheres. Sci. Rep. 7, 41260. https://doi.org/10.1038/srep41260.
Foltescu, V.L., Selin Lindgren, E., Isakson, J., Öblad, M., Tiede, R., Sommar, J., Pacyna, J.M., Toerseth, K., 1996. Airborne concentrations and deposition flixes of major and trace species at marine stations in southern Scandinavia. Atmos. Environ. 30, 3857–3872.
Gantt, B., Kelly, J.T., Bash, J.O., 2015. Updating sea spray aerosol emissions in the Community Multiscale Air Quality (CMAQ) model version 5.0.2. Geosci. Model Dev. (GMD) 8, 3733–3746.
Gimsenius, M.A., 1996. Regional and Seasonal Variations of Seassalt Aerosols in New South Wales, Australia. Thesis for Master's Degree in Physics. Department of Nuclear Physics, Lund University, Lund, Sweden.
Giorgi, F., 1988. Dry deposition velosities of atmospheric aerosols as inferred by applying a particle dry deposition parameterization to a general circulation model. Tellus 40B, 23–41.
Goto, M., Moriizumi, J., Yamazawa, H., Iida, T., Zhuo, W., 2008. Estimation of global radon exhalation rate distribution. In: Paschoa, A.S. (Ed.), The Natural Radiation Environment—8th International Symposium. American Institute of Physics, pp. 169–172.
Gondwe, M., Krol, M., Gieskes, W., Klaassen, W., de Barr, H., 2003. The contribution of ocean-leaving DMS to the global atmospheric burdens of DMS, MSA, SO2, and NSS $SO4^{=}$. Glob. Biogeochem. Cycles 17, 1056. https://doi.org/10.1029/2002GB001937.
Gustafsson, M.E.R., Franzén, L.G., 2000. Inland transport of marine aerosols in southern Sweden. Atmos. Environ. 34, 313–325.
Hallal, T., Box, G.P., Cohen, D.D., Stelcer, E., 2013. Size-resolved elemental composition of aerosol particles in greater Sydney in 2002-2003. Environ. Chem. 10, 295–305.
Hopkins, R.J., Desyaterik, Y., Tivanski, A.V., Zaveri, R.A., Berkowitz, C.M., Tyliszczak, T., Gilles, M.K., Laskin, A., 2008. Chemical speciation of sulfur in marine cloud droplets and particles: analysis of individual particles from the marine boundary layer over the California current. J. Geophys. Res. 113 D04209.
Hsu, Y.-K., Hilsen, T.M., Hopke, P.K., 2003. Comparison of hybrid receptor models to locate PCB sources in Chicago. Atmos. Environ. 37, 545–562.
Keene, W.C., Pszenny, A.A.P., Jacob, R.A., Duce, J.N., Galloway, J.N., Schultz-Tokos, J.J., Sievering, H., Boatman, J.F., 1990. The geochemical cycling of reactive chlorine through the marine troposphere. Glob. Biogeochem. Cycles 4, 407–430.
Knipping, E.M., Dabdub, D., 2003. Impact of chlorine emissions from sea-salt aerosol on coastal urban ozone. Environ. Sci. Technol. 37, 275–284.
Koffi, E.N., Bergamaschi, P., Karstens, U., Krol, M., Segers, A., Schmidt, M., Levin, I., Vermeulen, A.T., Fisher, R.E., Kazan, V., Klein Baltink, H., Lowry, D., Manca, G., Meijer, H.A.J., Moncrieff, J., Pal, S., Ramonet, M., Scheeren, H.A., H. A, Williams, A.G., 2016. Evaluation of the boundary layer dynamics of the TM5 model over Europe. Geosci. Model Dev. (GMD) 9, 3137–3160.
Levy, I., Mahrer, Y., Dayan, U., 2009. Coastal and synoptic recirculation affecting air pollutants dispersion: a numerical study. Atmos. Environ. 43, 1991–1999.
Marine Science, 2018. Accessed March 2018. http://www.marinebio.net/marinescience/02ocean/swcomposition.htm.
McInnes, L.M., Covert, D.S., Quinn, P.K., Germani, M.S., 1994. Measurement of chloride depletion and sulfur enrichment in individual sea-salt particles collected from the remote marine boundary layer. J. Geophys. Res. Atmos. 99, 8257. https://doi.org/10.1029/93JD03453.
Pio, C.A., Lopes, D.A., 1998. Chlorine loss from marine aerosol in a coastal atmosphere. J. Geophys. Res. 103 25,263-25,272.
Paatero, P., Tapper, U., 1994. Positive Matrix Factorisation: a non-negative factor model with optimal utilisation of error estimates of data values. Environmetrics 5, 111–126.
Paatero, P., 2004. User's Guide for Positive Matrix Factorisation Programs PMF2 and PMF3, Part 2: Reference. University of Helsinki, Helsinki, Finland.
Prijith, S.S., Aloysius, M., Mohan, M., 2014. Relationship between wind speed and sea salt aerosol production: a new approach. J. Atmos. Sol. Terr. Phys. 108, 34–40.
Quinn, P.K., Bates, T.S., 2005. Regional aerosol properties: comparisons of boundary layer measurements from ACE 1, ACE 2, Aerosols99, INDOEX, ACE Asia, TARFOX and NEAQS. J. Geophys. Res. 110, D14202. https://doi.org/10.1029/2004JD004755.
Riedel, T.P., Wolfe, G.M., Danas, K.T., Gilman, J.B., Kuster, W.C., Bon, D.M., Vladenko, A., Li, S.-M., Williams, E.J., Lerner, B.M., Veres, P.R., Roberts, J.S., Holloway, J.S., Lefer, B., Brown, S.S., Thornton, J.A., 2013. An MCM modeling study of nitryl chloride ($ClNO_2$) impacts on oxidation, ozone production and nitrogen oxide partitioning in polluted continental outflow. Atmos. Chem. Phys. 13, 28973–29006.
Road and Maritime Services, 2018. Traffic Volume Viewer. http://www.rms.nsw.gov.au/about/corporate-publications/statistics/traffic-volumes/aadt-map/index.html#/?z=6.
Schery, S.D., Wasiolek, M.A., 1998. Radon and thoron in the human environment, chap. In: Modeling Radon Flux from the Earth's Surface. World Scientific Publishing, Singapore, pp. 207–217.
Song, C.H., Carmichael, G.R., 1999. The aging process of naturally emitted aerosol (sea-salt and mineral aerosol) during long range transport. Atmos. Environ. 33, 2203–2218.
Stein, A.F., Draxler, R.R., Rolph, G.D., Stunder, B.J.B., Cohen, M.D., Ngan, F., Dec 2015. Free access NOAA's HYSPLIT atmospheric transport and dispersion modeling system. 2059-2077. Bull. Am. Meteorol. Soc. 2059–2077. https://doi.org/10.1175/BAMS-D-14-00110.1.
Taha, G., Box, G.P., Cohen, D.D., Stelcer, E., 2007. Black carbon measurement using laser integrating plate method. Aerosol Sci. Technol. 41, 266–276.
Zahorowski, W., Chambers, S., Henderson-Sellers, A., 2004. Ground based radon-222 observations and their application to atmospheric studies. J. Environ. Radioact. 76, 3–33.
Zhang, K., Wan, H., Zhang, M., Wang, B., 2008. Evaluation of the atmospheric transport in a GCM using radon measurements: sensitivity to cumulus convection parameterization. Atmos. Chem. Phys. 8, 2811–2832.